American Journal of Mechanical and Industrial Engineering
2023; 8(5): 110-122
http://www.sciencepublishinggroup.com/j/ajmie
doi: 10.11648/j.ajmie.20230805.11
ISSN: 2575-6079 (Print); ISSN: 2575-6060 (Online)

Active Control of Shaft Torsional Vibration with a Dynamic Torque Actuator

Luo Qing*, Fan Wen-kun, Hu Jie, Dong Jia-xin, Wang Jiao

Power Plant Division, Shanghai Marine Diesel Engine Research Institute, Shanghai, China

Email address:
dtfa_ll@126.com (Luo Qing)

*Corresponding author

To cite this article:
Luo Qing, Fan Wen-kun, Hu Jie, Dong Jia-xin, Wang Jiao. Active Control of Shaft Torsional Vibration with a Dynamic Torque Actuator. *American Journal of Mechanical and Industrial Engineering*. Vol. 8, No. 5, 2023, pp. 110-122. doi: 10.11648/j.ajmie.20230805.11

Received: September 17, 2023; **Accepted**: October 26, 2023; **Published**: November 9, 2023

Abstract: Torsional vibration is one of the critical areas of shafting vibration. Multi-harmonic fluctuations from the output torque of an engine, propeller, or other power sources constitute the main source of torsional vibration of a shafting system, and stimulate other coupled vibrations. Torsional dampers have been the main coutermeasure to deal with torsional vibration. However, with the increasing requirements for vibration and noise reduction, such traditional method has exposed obvious shortcomings. People have been researching for new technological methods, but seem to be in lack of significant breakthroughs. We attempts to Innovatively propose an systematical solution by both software and hardware. This paper introduces a new method to address torsional vibrations of shafting systems based on line spectrum active control. A multi-body dynamic analysis model is used to reveal the coupling characteristics of torsional vibration and vibration in other directions. In addition, a new cross-coupled multi-channel line spectrum active control algorithm is proposed alongside a new type of torque actuator where the internal electromagnetic structure contains a rotating stator and rotor. These components are connected with springs, and the whole assembly can rotate with the shafting. The dynamic torque is issued according to the command of the active control system in order to suppress the torque fluctuation caused by the power sources, which in turn greatly reduces the torsional vibration of the shafting.

Keywords: Torsional Vibration, Torque Fluctuation, Active Control Algorithm, Electromagnet, Torque Actuator, Multi-Body Dynamics, Vibrational Coupling

1. Introduction

The output torque of engines, propellers, and other power sources under operation often contain multi-harmonic fluctuations, which leads to shafting torsional vibration and can even induce other vibrations that couple with torsional vibration [1, 2]. The common countermeasure for torsional vibration of shafting is torsional vibration dampers. This is done to attenuate the torsional vibration amplitude at the resonance frequency of the shafting. Parameters such as moment of inertia, stiffness, and damping ratio of the damper are designed and tuned to maximize attenuation of torsional vibrations. Rubber torsional vibration dampers or oil-liquid torsional vibration dampers are widely used in engineering and can reduce effects of vibration frequencies that contain a prominent torsional vibration amplitude. The parameters of the semi-active magnetorheological fluid (MR) torsional vibration dampers, as its damping, can be adjusted based on shaft rotation speed to effectively reduce the resonance points at multiple speeds [3]. For new power systems equipped with motors, a feedback loop is constructed with the torque of the motor, and the modal parameters of the system are optimized by PID control to avoid coupling between the disturbance of the excitation source and the resonance frequency of the system [4]. However, even if the torsional resonance of the shafting is addressed, the multi-harmonic torsional vibrations excited by the engine and other coupled vibrations [5] still introduce challenges in maintaining quietness and concealment in many real-world use cases.

Active noise and vibration control principles were put forward as early as the 1930s. More recently, with the development of digital signal processing technology and high-performance computing as well as the development of

high-precision sensors and actuators with stable performance, active noise and vibration control technologies have been used widely across many industries. As one of the core parts of active noise and vibration control technology, active control algorithms have matured after decades of development. The representative methods include optimum control, robust control, adaptive control, intelligent control, etc. LMS (Least Mean Square) algorithm and its extended self-adaptive control algorithm are the most widespread in line spectrum vibration control. As early as the 1980s, Widrow et al. proposed a notch filter with two adaptive weight coefficients to eliminate external harmonic interference [6]. Subsequently, the Fx LMS algorithm was proposed and widely used in industry [7]. Based on the Fx LMS algorithm and as a promotion of the Fx LMS algorithm, Elliott et al. proposed a multi error LMS algorithm to attenuate the lumped error. [8]. Cabell et al. researched the core algorithm of active noise control for twin turboprop aircraft on the basis of Fx LMS algorithm [9]. Chang et al. researched the Fx LMS algorithm with variable step size in order to obtain faster convergence speed and better control effect [10]. Kim et al. proposed an active noise control structure using an adaptive notch filter to estimate frequency online [11]. Zhang et al. researched an adaptive control algorithm using tracking filters to control the disturbance of periodic frequency fluctuations [12].

This paper presents a new method to solve the torsional vibration of shafting based on active line spectrum control. Firstly, a multi-body dynamic model is analyzed to show that the generalized motion of shafting in all directions, including rotation and translation in space, has coupling characteristics. The model reveals that the suppression of torsional vibration should reduce coupled vibrations, which is of great practical significance. Secondly, following the characteristics of multi-harmonic vibration active control systems for complex shafting that may be equipped with several actuators, a new cross-coupled multi-channel line spectrum active control algorithm is introduced. Finally, a new electromagnetic dynamic torque actuator that is rigidly connected to the shafting system is presented. The actutator sends out dynamic torque with the same frequency and opposite phase to the torsional vibration of the shafting system according to the command of the active controller and algorithm to achieve a high reduction in the torsional vibration of the shaft system.

2. Multi-Body Dynamics Analysis of Shafting

A ship shafting system is composed of many parts, such as an engine and its accessories, mountings, bearings, couplings, transmission shafts, a gearbox, a propeller, etc. Multi-body dynamics analysis regards each component as a single body connected with each other through constraints. We first establish the general coordinate system of the shaft system and then establish the local coordinate system fixed with the body. Assume that the shaft system contains n_b bodies. The position of any point P on the ith body in the total coordinate can be expressed as [13].

$$r^i = R^i + A^i u^i, i = 1, 2, \cdots, n_b \quad (1)$$

Where R^i is the position vector of the origin of the body i coordinate system in the general coordinate system. u^i is the coordinate vector of point P in the body coordinate system. A^i is the transformation matrix from the body coordinate system to the general coordinate system [13].

If the body is regarded as a rigid body, u^i will remain unchanged during the movement of the body, while R^i and A^i will vary along with the change of the body position. Therefore, the orientation parameters R^i and A^i of the body coordinate system determines the position state of the whole body. The coordinate system transformation A^i can be achieved by rotating the coordinate system of body i by an angle θ^i about an axis in the general coordinate system, so A^i reflects the rotation of the body i coordinate system, and R^i represents its translation. To simplify the subsequent matrix operation, a set of rotational parameters θ^i is used to represent the generalized rotation coordinate of the body i coordinate system. θ^i is the function of the body coordinate system azimuth θ^i. So the element of A^i can be expressed as the function of elements of θ^i.

If the body is taken as an elastic one, the finite element mesh is divided for the purpose of analyzing the elastic deformation of the body [14]. The body coordinate vector of any point P in the j[th] finite element of body i can be expressed as [13].

$$u^{ij} = N^{ij} B_1^{ij} q^i = N^{ij} B_1^{ij} \left(q_0^i + \underline{q_f^i}\right) = N^{ij} B_1^{ij} \left(q_0^i + B_2^i q_f^i\right) \quad (2)$$

Where N^{ij} is the shape function of element j (including the transformation matrix between body coordinate system and element coordinate system). q^i is the vector of all the nodes on the body, which merges the common nodes of adjacent elements. B_1^{ij} converts the node q^i of body i to the node on the element j. q_0^i is the undeformed local position of q^i node vector, which does not change with time in the body coordinate system. $\underline{q_f^i}$ is the state of elastic deformation of a node vector which is the quantity that changes with time during vibration. q_f^i is the coordinate vector of node elastic deformation. B_2^i can be regarded as the constraint condition related to elastic deformation, which is applied to q_f^i to eliminate the freedom of rigid body motion and obtain the unique elastic deformation [13].

Substituting Equation (2) into Equation (1), the general coordinate position vector of any point P in element j on body i is expressed as:

$$r^{ij} = R^i + A^i u^{ij} = R^i + A^i N^{ij} B_1^{ij} \left(q_0^i + B_2^i q_f^i\right) \quad (3)$$

Calculate the speed of r^{ij} from Equation (3)

$$\dot{r}^{ij} = \dot{R}^i + \dot{A}^i u^{ij} + A^i \dot{u}^{ij} = \dot{R}^i + B^{ij} \dot{\theta}^i + A^i N^{ij} B_1^{ij} B_2^i \dot{q}_f^i = \left[I \; B^{ij} \; A^i N^{ij} B_1^{ij} B_2^i \right] \left[\dot{R}^i \; \dot{\theta}^i \; \dot{q}_f^i \right]^T \quad (4)$$

Where $\left[\dot{R}^i\ \dot{\theta}^i\ \dot{q}_f^i\right]^T$ is the generalized coordinate velocity vector, which respectively expresses the rigid body translation and rotation of the body coordinate system and the elastic deformation of the body finite element node. I is the identity matrix. By means of B^{ij} (which is combination of matrices), realize the conversion from $\dot{A}^i$ to the generalized rotational coordinate velocity $\dot{\theta}^i$ [13]. In regard to 2-dimensional plane, the body frame can only rotate about the Z axis of the general coordinates, so $\dot{A}^i$ is equal to the partial derivative of A^i with respect to θ^i multiplied by $\dot{\theta}^i$

Using Equation (4), the kinetic energy of the j[th] finite element of body i can be expressed as [13].

$$T^{ij} = \frac{1}{2}\int_{V^{ij}} \rho^{ij} \dot{r}^{ij^T} \dot{r}^{ij} dV^{ij} \tag{5}$$

Where ρ^{ij} is the mass density of the element and V^{ij} is the volume of the element.

Substituting Equation (4) into Equation (5), it can be deduced

$$T^{ij} = \frac{1}{2}\dot{q}^{i^T} M^{ij} \dot{q}^i \tag{6}$$

Where M^{ij} is the mass matrix of the element. Let the number of elements on body i be n_e, and the kinetic energy of body i is [13].

$$\mathrm{T^i} = \sum_{\mathrm{j=1}}^{\mathrm{n_e}} \mathrm{T^{ij}} = \frac{1}{2}\sum_{\mathrm{j=1}}^{\mathrm{n_e}} \dot{\mathrm{q}}^{\mathrm{i}^T} \mathrm{M^{ij}} \dot{\mathrm{q}}^{\mathrm{i}} = \frac{1}{2}\ \dot{\mathrm{q}}^{\mathrm{i}^T} \left[\sum_{\mathrm{j=1}}^{\mathrm{n_e}} \mathrm{M^{ij}}\right]\ \dot{\mathrm{q}}^{\mathrm{i}} = \frac{1}{2}\dot{\mathrm{q}}^{\mathrm{i}^T} \mathrm{M^i} \dot{\mathrm{q}}^{\mathrm{i}} \tag{7}$$

Where the mass matrix of body can be expanded as

$$\mathrm{M^i} = \begin{bmatrix} \mathrm{M^i_{RR}} & \mathrm{M^i_{R\theta}} & \mathrm{M^i_{Rf}} \\ \mathrm{M^i_{\theta R}} & \mathrm{M^i_{\theta\theta}} & \mathrm{M^i_{\theta f}} \\ \mathrm{M^i_{fR}} & \mathrm{M^i_{f\theta}} & \mathrm{M^i_{ff}} \end{bmatrix} \tag{8}$$

M^i is a symmetric matrix. In the formula (8), M^i_{RR} is a diagonal matrix, and the elements on its main diagonal are the mass of a body. The matrices $M^i_{R\theta}$ and $M^i_{\theta R}$ reflect the mass coupling between translational and rotational body coordinate systems. M^i_{Rf} and M^i_{fR} reflect the mass coupling between translational and elastic deformation of the coordinate system. $M^i_{\theta f}$ and $M^i_{f\theta}$ represent the mass coupling between rotational and elastic deformation of the coordinate system. It is worth pointing out that $M^i_{\theta\theta}$ and $M^i_{R\theta}(M^i_{\theta R})$ are related not only to the generalized rotational and translational coordinates of the coordinate system but also to the generalized elastic coordinates. As a result, the mass coupling between translational and rotational motion (vibration) will be inevitable in a general sense [13].

Since the parts of the shafting system are connected together by various constraints, the Lagrange equation with constraint conditions should be used. For body i, it can be deduced from the virtual work principle [13].

$$\frac{\mathrm{d}}{\mathrm{dt}}\left(\frac{\partial \mathrm{T^i}}{\partial \dot{\mathrm{q}}^{\mathrm{i}}}\right)^{\mathrm{T}} - \left(\frac{\partial \mathrm{T^i}}{\partial \mathrm{q^i}}\right)^{\mathrm{T}} + \mathrm{C^T_{q^i}}\lambda = -\mathrm{K^i q^i} + \mathrm{Q^i_e} \tag{9}$$

Where

K^i is the finite element elastic stiffness matrix of body i, which just depends on $\dot{q}_f^i$. Its expanded form can be expressed as

$$K^i = \begin{bmatrix} 0 & & \\ & 0 & \\ & & K^i_{ff} \end{bmatrix}$$

K^i_{ff} usually contains components related to the translation and rotation of elastic deformation, and there is a coupling relationship between them in general [15, 16].

Q_e^i is the external force exerted on body i, and its subitems are [13].

$$\mathrm{Q^i_e} = [(\mathrm{Q^i_e})_R \quad (\mathrm{Q^i_e})_\theta \quad (\mathrm{Q^i_e})_f]^{\mathrm{T}}$$

Where $(Q_e^i)_R$ is the generalized force associated with the translational movement of the body coordinate system, $(Q_e^i)_\theta$ is the generalized force associated with the rotation of the coordinate system, and $(Q_e^i)_f$ is the generalized force acting on the elastic deformation coordinates of the body i.

$C_{q^i}^T$ is the Jacobian matrix of the constraint equation on body i.

The constraint equation can be expressed as [13].

$$\mathrm{C(q^i, t)} = \left[\mathrm{C_1(q^i, t)} \quad \mathrm{C_2(q^i, t)} \quad \cdots \quad \mathrm{C_{n_c}(q^i, t)}\right]^{\mathrm{T}} = 0, n_c \textit{ is the number of linear independent constraint equations for body } i$$

the Jacobian matrix of the constraint equation [13].

$$\mathrm{C_{q^i}} = \frac{\partial \mathrm{C}}{\partial \mathrm{q^i}} = \left[\frac{\partial \mathrm{C_1}}{\partial \mathrm{q^i}} \quad \frac{\partial \mathrm{C_2}}{\partial \mathrm{q^i}} \quad \cdots \quad \frac{\partial \mathrm{C_{n_c}}}{\partial \mathrm{q^i}}\right]^{\mathrm{T}}$$

$\lambda = \left[\lambda_1\ \lambda_2\ \cdots\ \lambda_{n_c}\right]^T$, the vector of Lagrange multipliers.

Substitute Equation (7) into Equation (9) to obtain Newton's dynamic equation [13].

$$\mathrm{M^i \ddot{q}^i + K^i q^i = Q^i_e + Q^i_v - C^T_{q^i}\lambda} \tag{10}$$

In the above equation, Q_v^i is called the quadratic velocity vector, that is, the inertial force related to the product of the generalized coordinate velocity vector, which is caused by coordinate rotation, including centrifugal forces and Coriolis forces. Centrifugal forces are essential for analyzing the imbalance of the rotating shaft [16], and Coriolis forces are closely related to the gyroscopic effect of some rotating parts [17], which forms dynamic forces and causes relevant vibration [18, 19].

In a vibration study of shafting, it is evidently appropriate to introduce the concept of vibration modal analysis study. According to the modal analysis theory, for a linear time-invariant system, the response of any point in the system

can be expressed as a linear combination of modes of various order [13]. Hence there are:

$$\mathrm{q_f^i} = \mathrm{B_m^i q_m^i}$$

Where q_m^i is the node modal coordinate vector, B_m^i is a transformation matrix composed of modal mode vectors, which transforms the physical coordinates of elastic deformation of nodes (subscript f) into modal coordinates (subscript m). Using modal coordinates, Equation (10) becomes

$$\begin{bmatrix} \mathrm{M_{RR}^i} & \mathrm{M_{R\theta}^i} & \mathrm{M_{Rm}^i} \\ \mathrm{M_{\theta R}^i} & \mathrm{M_{\theta\theta}^i} & \mathrm{M_{\theta m}^i} \\ \mathrm{M_{mR}^i} & \mathrm{M_{m\theta}^i} & \mathrm{M_{mm}^i} \end{bmatrix} \begin{bmatrix} \ddot{\mathrm{R}}^{\mathrm{i}} \\ \ddot{\theta}^{\mathrm{i}} \\ \ddot{\mathrm{q}}_{\mathrm{m}}^{\mathrm{i}} \end{bmatrix} + \begin{bmatrix} 0 & & \\ & 0 & \\ & & \mathrm{K_{mm}^i} \end{bmatrix} \begin{bmatrix} \mathrm{R}^{\mathrm{i}} \\ \theta^{\mathrm{i}} \\ \mathrm{q}_{\mathrm{m}}^{\mathrm{i}} \end{bmatrix} = [(Q_e^i)_R \ (Q_e^i)_\theta \ (Q_e^i)_m \ ]^T + [(Q_v^i)_R \ (Q_v^i)_\theta \ (Q_v^i)_m \ ]^T - \left[C_{R^i}^T \ C_{\theta^i}^T \ C_{q_m^i}^T \right]^T \lambda \quad (11)$$

Combine all vectors of bodies in the shafting into a total dynamic equation [13].

$$\mathrm{M\ddot{q} + Kq = Q_e + Q_v - C_q^T \lambda} \quad (12)$$

Where

$$\mathrm{M} = \begin{bmatrix} \mathrm{M}^1 & & & \\ & \mathrm{M}^2 & & 0 \\ & & \ddots & \\ 0 & & & \mathrm{M}^{\mathrm{n_b}} \end{bmatrix}, \ \mathrm{K} = \begin{bmatrix} \mathrm{K}^1 & & & \\ & \mathrm{K}^2 & & 0 \\ & & \ddots & \\ 0 & & & \mathrm{K}^{\mathrm{n_b}} \end{bmatrix}, \ \mathrm{q} = \begin{bmatrix} \mathrm{q}^1 \\ \mathrm{q}^2 \\ \vdots \\ \mathrm{q}^{\mathrm{n_b}} \end{bmatrix}$$

$$\mathrm{C_q^T} = \begin{bmatrix} \mathrm{C_{q^1}^T} \\ \mathrm{C_{q^2}^T} \\ \vdots \\ \mathrm{C_{q^{n_b}}^T} \end{bmatrix}, \ \mathrm{Q_e} = \begin{bmatrix} \mathrm{Q_e^1} \\ \mathrm{Q_e^2} \\ \vdots \\ \mathrm{Q_e^{n_b}} \end{bmatrix}, \ \mathrm{Q_v} = \begin{bmatrix} \mathrm{Q_v^1} \\ \mathrm{Q_v^2} \\ \vdots \\ \mathrm{Q_v^{n_b}} \end{bmatrix}$$

It can be difficult to find a closed-form solution to Equation (12). Therefore, the time differential of both sides of the constraint square $C(q,t) = 0$ is calculated twice and sorted out to generate the acceleration equation form of constraints [20].

$$\mathrm{C_q \ddot{q} = \gamma} \quad (13)$$

Combine Equation (12) and Equation (13) into an equation to obtain

$$\begin{bmatrix} \mathrm{M_{rr}} & \mathrm{M_{rm}} & \mathrm{C_{q_r}^T} \\ \mathrm{M_{mr}} & \mathrm{M_{mm}} & \mathrm{C_{q_m}^T} \\ \mathrm{C_{q_r}} & \mathrm{C_{q_m}} & 0 \end{bmatrix} \begin{bmatrix} \ddot{\mathrm{q}}_{\mathrm{r}} \\ \ddot{\mathrm{q}}_{\mathrm{m}} \\ \lambda \end{bmatrix} = \begin{bmatrix} \mathrm{Q_r} \\ \mathrm{Q_m} \\ \gamma \end{bmatrix} \quad (14)$$

Where, $q_r = [R \ \theta \ ]^T$ represents the translation and rotation generalized coordinate vectors of all body coordinate systems.. q_m represents the elastic deformation modal coordinate vector of all bodies. All items in the matrix are classified and summarized according to the coordinates of q_r and q_m. $K_{mm}q_m$ (generalized elastic forces) is included in Q_m.

Given a set of initial conditions, the acceleration value of the generalized coordinate can be obtained by solving Equation (14), and then the velocities along with the coordinates can be obtained through integration [13].

The output power of excitation sources that has a shafting, such as an engine, contains prominent torque fluctuations which has a significant impact on the vibration and noise of the shafting and its surroinding environment [21, 22]. These dynamic torques can be classified as the generalized rotational force of rigid body rotation $(Q_e)_\theta$, and also the elastic generalized force $(Q_e)_f$ or Q_m. Equations (10) to (14) show that through the coupling effect between different coordinates in the mass matrix M^i and the elastic stiffness matrix K^i, the dynamic torques can cause vibration in translational directions, and at the same time, the vibration is transmitted to different parts of the shafting by way of the constraints between bodies.

The active control torque provided by a dynamic torque actuator can be arranged at the position where the influence of torque fluctuation has to be offset. Correspondingly this control torque is added into Q_e and/or Q_m in Equation (11) or (14). This not only directly reduce the torsional vibration, but also effectively reduce the vibration in other directions with the help of the coupling effect. SIEMENS Motion platform provides an excellent simulation environment for this purpose and an opportunity to carry out in-depth analysis and optimization.

3. Active Vibration Control Algorithm of Multi-Channel Cross-Coupled Line Spectrum

The schematic diagram of multi-channel active control is shown in Figure 1, illustrated using a two-channel example which take into account the cross interference between control channels. F_a and F_p represent the control force and disturbance force respectively. H_a^a and H_a^p represents the frequency response function matrix of control channel and disturbance channel respectively. H_k^a and H_k^p represents the frequency response function matrix between the active control force, disturbance force and the end response point of the control point respectively. A_a and A_k represents the acceleration of the error response point and the end response

point respectively. The digital subscripts and superscripts represent the number of the corresponding control points and error response points respectively.

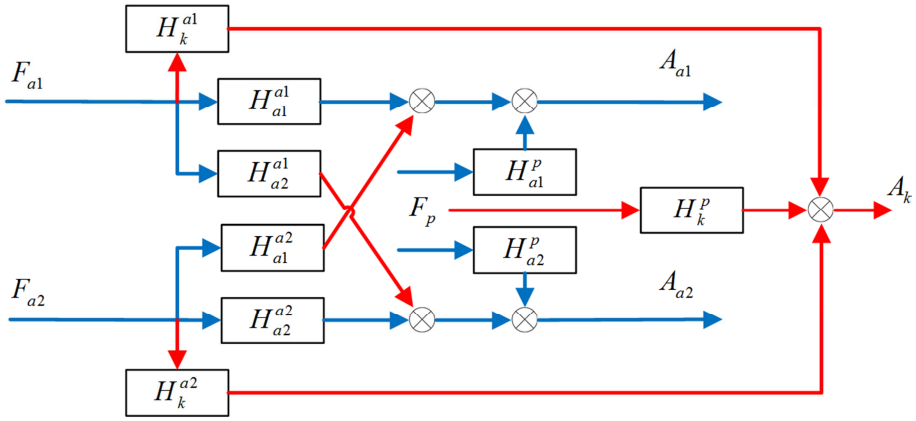

Figure 1. *Schematic diagram of multi-channel coupled active control (2 channels as an example).*

It is assumed that under ideal control, the active control force of each control point can suppress the acceleration of each error response point to zero, as shown in Equation (15)

$$\begin{bmatrix} A_{a1} \\ A_{a2} \\ \vdots \\ A_{aN} \end{bmatrix} = \begin{bmatrix} H_{a1}^{a1} & H_{a1}^{a2} & \cdots & H_{a1}^{aN} \\ H_{a2}^{a1} & H_{a2}^{a2} & \cdots & H_{a2}^{aN} \\ \vdots & \vdots & & \vdots \\ H_{aN}^{a1} & H_{aN}^{a2} & \cdots & H_{aN}^{aN} \end{bmatrix} \begin{bmatrix} F_{a1} \\ F_{a2} \\ \vdots \\ F_{aN} \end{bmatrix} + \begin{bmatrix} H_{a1}^{P} \\ H_{a2}^{P} \\ \vdots \\ H_{aN}^{P} \end{bmatrix} F_P = 0 \quad (15)$$

From Equation (15), the ideal control force expression of each control point can be calculated as

$$\begin{bmatrix} F_{a1} \\ F_{a2} \\ \vdots \\ F_{aN} \end{bmatrix}_{ideal} = - \begin{bmatrix} H_{a1}^{a1} & H_{a1}^{a2} & \cdots & H_{a1}^{aN} \\ H_{a2}^{a1} & H_{a2}^{a2} & \cdots & H_{a2}^{aN} \\ \vdots & \vdots & & \vdots \\ H_{aN}^{a1} & H_{aN}^{a2} & \cdots & H_{aN}^{aN} \end{bmatrix}^{-1} \begin{bmatrix} H_{a1}^{P} \\ H_{a2}^{P} \\ \vdots \\ H_{aN}^{P} \end{bmatrix} F_P \quad (16)$$

The acceleration of the end response is expressed as

$$A_k = H_k^P F_P + \sum_{i=1}^{N} \left(H_k^{ai} F_{ai} \right) \ (i = 1, 2, \cdots, N) \quad (17)$$

The online identification method of target line spectrum is shown in Figure 2 below. The superscript * of some parameters in the figure represents the real-time estimated values. The estimated error signal e*(t) is fed back to controller C, and the control signal u (t) generated by the controller excites system P to generate a response y(t) to cancel the external disturbance d(t). The goal of the control algorithm is to make the system response y(t) infinitely close to - d(t). System P is assumed to be a stable time-invariant system at one location. Generally, the target line spectrum of the controlled signal d(t) is known. The online identification algorithm needs to calculate the real part and imaginary part of system P in real time.

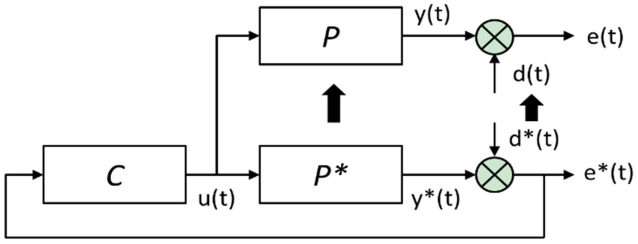

Figure 2. *Schematic Diagram of Target Line Spectrum Online Identification Algorithm.*

It can be seen from Figure 2 that e(t)=P [u(t)]+d(t), where P [u(t)] represents the time domain response generated after the control signal u(t) excites system P.

Assuming that the external interference is a harmonic signal, d*(t) can be expressed as

$$d^*(t) = d_c^* cos\ (\omega t)\ + d_s^* sin\ (\omega t) \quad (18)$$

Where ω is the original frequency of the disturbance signal.

Under steady-state excitation, the control signal u(t) should be a harmonic signal with the same frequency as the disturbance signal.

$$u(t) = u_c cos\ (\omega t)\ + u_s sin\ (\omega t) \quad (19)$$

In combination with e(t) expression, there is

$$e(t) \backsimeq e^*(t) = \begin{bmatrix} cos(\omega t) \\ sin(\omega t) \end{bmatrix}^T \left\{ \begin{bmatrix} P_R^* & P_I^* \\ -P_I^* & P_R^* \end{bmatrix} \begin{bmatrix} u_c \\ u_s \end{bmatrix} + \begin{bmatrix} d_c^* \\ d_s^* \end{bmatrix} \right\} = (P_R^* u_c + P_I^* u_s + d_c^*)\ cos\ (\omega t)\ + (-P_I^* u_c + P_R^* u_s + d_s^*)\ sin\ (\omega t) \quad (20)$$

Where P_R^* and P_I^* represent the real and imaginary parts of the system frequency response when the frequency is ω, respectively. To minimize the objective function $J = \varepsilon^2(t) / 2 = [e^*(t) - e(t)]^2 / 2$, the gradient descent algorithm is used to estimate two unknown parameters, and the recursive form of the estimation formula is

$$\begin{cases} \dot{P}_R^* = -g[u_c\ cos(\omega t) + u_s\ sin(\omega t)]\varepsilon(t) \\ \dot{P}_I^* = -g[u_s\ cos(\omega t) - u_c\ sin(\omega t)]\varepsilon(t) \end{cases} \quad (21)$$

Where g represents an updating iteration step size, which affects the search speed of the algorithm, and usually has a small value to ensure the stability of the algorithm.

By utilizing an online target line spectrum identification algorithm and building upon the principles of multi-channel coupled active control, a multi-channel harmonic adaptive global control method is developed, which takes into account the cross coupling between control channels. Compared to a single-channel control system, a multi-channel system is characterized by coupling between its channels. Specifically the non-diagonal element of the system transfer matrix is not zero. The purpose of the multi-channel cross-coupling algorithm is to address the cross coupling between different channels in the weight-updating stage of the control output so as to realize the adaptive global control of multiple channels. Illustrating with a two-channel example, Figure 3 includes the cross-coupling elements (P_{12} and P_{21}) between the control channels. In other words, the algorithm takes into account the non-diagonal elements of the system transfer matrix, incorporating all elements of the matrix into the algorithm. In the figure, the superscript * represents the real-time estimated values, and the subscript of the parameters represents the control channel number.

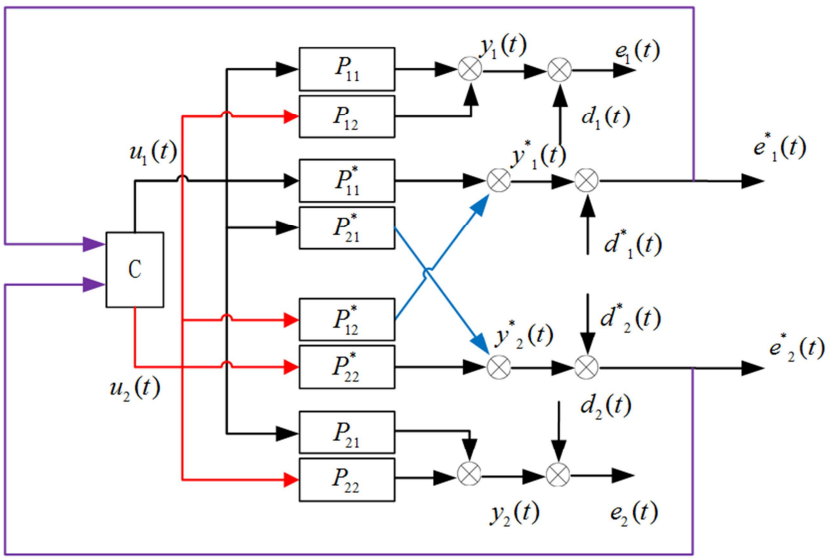

Figure 3. *Time domain multi-channel active control algorithm.*

The N-channel harmonic adaptive control method is derived. If the external disturbance is still assumed to be a harmonic signal, then the control signal should also be a harmonic signal of the same frequency. Estimated error signal e*t can be expressed as

$$e^*(t) = W^T(G^*U^* + D^*) \tag{22}$$

Where

$$W = \begin{bmatrix} cos(\omega t) & & & \\ sin(\omega t) & & & \\ & cos(\omega t) & & \\ & sin(\omega t) & & \\ & & \dots & \\ & & \dots & \\ & & & cos(\omega t) \\ & & & sin(\omega t) \end{bmatrix}$$

$$U^* = [u_{c1}^* \; u_{s1}^* \; u_{c2}^* \; u_{s2}^* \; \dots u_{cN}^* \; u_{sN}^* \;]^T$$

$$D^* = [d_{c1}^* \; d_{s1}^* \; d_{c2}^* \; d_{s2}^* \; \dots d_{cN}^* \; d_{sN}^* \;]^T$$

$$G^* = \begin{bmatrix} P_{R11}^* & P_{I11}^* & P_{R12}^* & P_{I12}^* & \cdots & P_{R1N}^* & P_{I1N}^* \\ -P_{I11}^* & P_{R11}^* & -P_{I12}^* & P_{R12}^* & \cdots & -P_{I1N}^* & P_{R1N}^* \\ \vdots & \vdots & & & & & \vdots \\ P_{RN1}^* & P_{IN1}^* & P_{RN2}^* & P_{IN2}^* & \cdots & P_{RNN}^* & P_{INN}^* \\ -P_{IN1}^* & P_{RN1}^* & -P_{IN2}^* & P_{RN2}^* & \cdots & -P_{INN}^* & P_{RNN}^* \end{bmatrix}$$

Where the numerical subscripts of P_R^* and P_I^* represent the response point (first digit) and the excitation point (second digit) respectively. The subscript of u_c^*, u_s^*, d_c^*, and d_s^* indicates the number of control channels. It can be seen from the matrix G^* that the multi-channel control algorithm that does not consider cross-coupling only calculates diagonal elements in the matrix, while the multi-channel suppression method that takes cross-coupling will calculate all elements in the matrix.

The unknown parameters P_R^*, P_I^*, d_c^* and d_s^* are estimated by gradient descent, and the recursive form is as follows

$$\begin{cases} \dot{P}_{Rij}^* = -g\left[u_{cj}^* cos(\omega t) + u_{sj}^* sin(\omega t)\right]\varepsilon_i(t) \\ \dot{P}_{Iij}^* = -g\left[u_{sj}^* cos(\omega t) + u_{cj}^* sin(\omega t)\right]\varepsilon_i(t) \\ \dot{d}_{ci}^* = -gcos(\omega t)\varepsilon_i(t) \\ \dot{d}_{si}^* = -gsin(\omega t)\varepsilon_i(t) \end{cases} \tag{23}$$

$$[e_i^*(t)]^2/2 \tag{24}$$

Where g represents the updating iteration constant, which affects the search speed of the algorithm and usually takes a small value to ensure the stability of the algorithm.

After the unknown parameters P_R^*, P_I^*, d_c^*, and d_s^* are

estimated, the values of control signal parameters u_{cj}^* and u_{sj}^* need to be solved. In order to avoid the difficulty of inversion, the gradient descent algorithm is used to minimize the objective function $\frac{[e_i^*(t)]^2}{2}$ for estimation, and then the recursive form of control signal parameters can be obtained

$$\begin{cases} u_{cj}^* = -g_u\left[P_{Rjj}^* \cos(\omega t) - P_{Ijj}^* \sin(\omega t)\right] e_j^*(t) \\ u_{sj}^* = -g_u\left[P_{Ijj}^* \cos(\omega t) + P_{Rjj}^* \sin(\omega t)\right] e_j^*(t) \end{cases} \quad (25)$$

Where g_u is the updating iteration constant.

4. Dynamic Torque Actuator

Figure 4 depicts the schematic diagram of the output torque of the actuator. The iron ring shown in the diagram, is located between the inner magnetic block and the outer magnetic block. Both magnetic blocks have radial magnetic fields that are oriented opposite one another towards the center of the iron ring. The coil is wound on iron ring. The two sections of wires (along the axial direction) that sit in the gap between the iron ring and the inner magnetic block and between the iron ring and the outer magnetic block are situated perpendicular to the magnetic force line. According to Ampere law, a tangential electromagnetic force (ampere force) is generated when a current is applied through the wire, and the ampere forces of the two coils in the same direction together produce torque around the axis center. This is the electromagnetic mechanism of the output torque of the actuator.

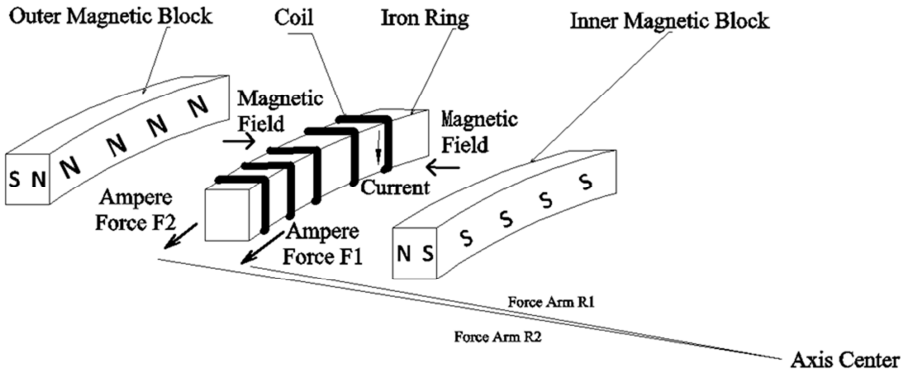

Figure 4. *Schematic Diagram of Actuator Output Torque.*

Figure 5 is a schematic diagram of the end face of the structure. The inner magnetic block and the outer magnetic block are fixed on the magnetic conductors respectively. The excitation current and magnetic field result in, the coil, together with the iron ring, oscillates clockwise or counterclockwise around the axis center, and outputs dynamic torque. By arranging this electromagnetic structure symmetrically along the circumference, pure torque output can be obtained. It should be noted that the end face portion of the coil will be influenced by the axial magnetic flux leakage which produces a negative torque, but the density of the magnetic flux leakage is one order of magnitude smaller than the radial magnetic field. Additionally, since the length of this portion of the coil is very short compared to the axial portion, the influence of the negative torque is very limited [23].

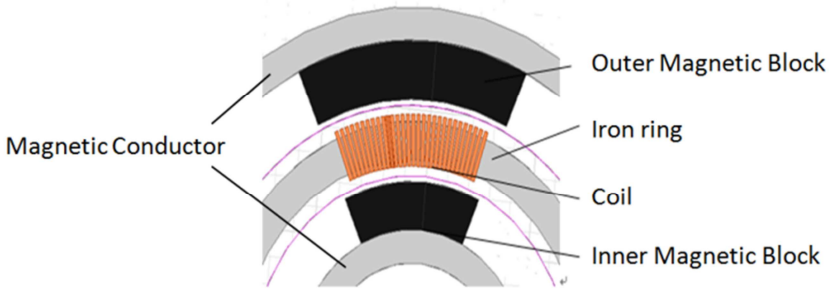

Figure 5. *Schematic Diagram of End Face Layout of Actuator.*

Figure 6 shows a sectional view of the structure of the actuator that rotates as a whole. The spindle and the magnetic conductors are fixed together, and both ends of the spindle are fixed to the shafting through connecting flanges 1 and 2 to rotate synchronously with the shafting. The coil-wrapped iron ring, which is located between the inner and outer magnetic block, is supported on the spindle through bearing 1 and bearing 2. The iron ring is also connected to the spindle by a springs (not shown in the figure) so that the coil-wrapped iron ring can not only oscillate slightly relative to the magnetic block (counterclockwise or clockwise) but also rotate along with the spindle and the shafting. When supplied with a control current, the coil generates a dynamic torque by interacting with the magnetic field. The torgue is subsequently transmitted to the spindle through the magnetic conductors and springs, which in turn exert torques on the shafting via

connecting flanges 1 and 2. This assembly enables the active control torque out of the actuator [24]. Since the actuator rotates along with the shaft system as a whole, it is necessary to transfer the external control current to the coil using a conductive slip ring.

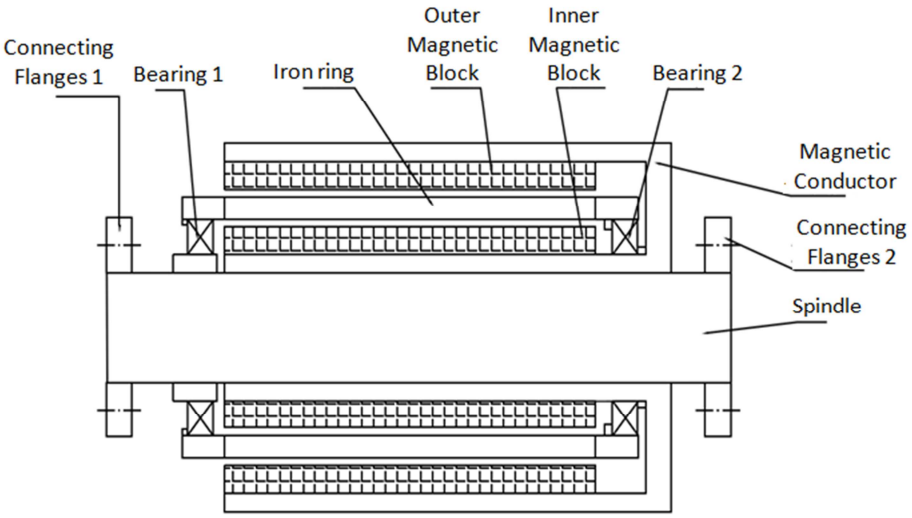

Figure 6. *Mechanical Structure Diagram of Actuator.*

According to Ampere's Law, the torque (M) generated by the energized coil of the actuator in the magnetic field can be expressed as:

$$M = \left(\int_{L_1} B_1 dl\right) iR_1 + \left(\int_{L_2} B_2 dl\right) iR_2 - \left(\int_{L_3} B_3 R_3 dl\right) i \quad (26)$$

Where, B_1 is the radial magnetic flux density perpendicular to the coil in the air gap at the inner side of the iron ring, which has a length of L_1. The former is a function of the coordinates of the latter. B_2 is the radial magnetic flux density perpendicular to the coil in the air gap at the outside of the iron ring, which has a length of L_2. Likewise, the former is a function of the coordinates of the latter. B_3 is the axial magnetic flux intensity, regarded as magnetic leakage, perpendicular to the coil at the two end faces of the iron ring, which is a function of the coordinates of this part of the coil. L_3 is defined as the length of the coil at the two end faces of iron ring. i is the excitation current intensity and is provided by the active control system. R_1 is the radius (force arm) between the L_1 inner side coil on the iron ring and the shaft center of the actuator, and R_2 is the radius (force arm) between the L_2 outer side coil on the iron ring and the shaft center of the actuator. R_3 is the radius between the two end face coil (L_3) on the iron ring and the shaft center of the actuator, which are a function of this part of the coil coordinates.

When the sizes of the coil winding structure and magnetic field distribution of the actuator are determined, the output torque of the actuator depends on the control current i and coil position (angle). If the magnetic field B remains unchanged within the rotation range of the coil, the ampere force torque is completely determined by the current i [25]. Depending on the signal type of i, the actuator can output various types of dynamic torque such as sines, impacts, broadband random, complex cycles, etc.

As mentioned above, the magnetic block and the spindle are rigidly fixed together, which is referred to as the stator. The coil-wrapped iron ring which can rotate relative to the magnetic block, constrained by the spring, is referred to as the rotor. The moment of inertia of the rotor is defined as be J. The dynamic angle of the rotor relative to the stationary foundation is defined as φ and the dynamic angle relative to the stator is defined as φ'. The electromagnetic torque M, as given by Equation (26), applied to the rotor and can be expressed using Newton's Second Law as shown below:

$$M = J \cdot \frac{d^2\varphi}{dt^2} + C \cdot \frac{d\varphi'}{dt} + K \cdot \varphi' \quad (27)$$

where k is the stiffness of the spring and C is its damping coefficient.

Since the reverse of force is equal to the reactive force, the electromagnetic torque received by the stator is - M, the spring force to the stator is Kφ', and the damping force to the stator is $C\frac{d\varphi'}{dt}$. The dynamic acting torque of the actuator received by the shafting is [26].

$$M_{active} = -M + C \cdot \frac{d\varphi'}{dt} + K \cdot \varphi' = -J \cdot \frac{d^2\varphi}{dt^2} \quad (28)$$

The actuator rotates along with the shafting system at high speeds, in the meantime there is a relative variable speed rotation between the magnetic block and the coil. It is necessary to investigate the influence of this compound movement on the actuator. The acceleration of any point A on the rotor, a_A, can be written as the vector sum of the relative acceleration a_r, the convected acceleration a_e, and the Coriolis acceleration a_k as

$$a_A = a_r + a_e + a_k$$

a_e reflects the effect of shafting movement on the actuator. The radial component of a_e is perpendicular to the rotation

direction of the rotor. If the rotor has sufficient stiffness and strength, its rotation will not be affected, neither will its output dynamic torque. The tangential component a_e is collinear with the rotation direction of the rotor. As a result, the stator imparts a tangential inertial force on the spring.

Simultaneously, the tangential component a_r causes the rotor to exert an inertial force on the spring. The spring should have an appropriate stiffness to prevent the rotor from frequently hitting the caging device and impairing its function.

a_k, the Coriolis acceleration, can be expressed as

$$a_k = 2\omega \times v_r$$

where ω is the angular velocity vector of the stator, that is, the rotational angular velocity of the spindle. Given that the rotor's only relative motion concerning the stator is its rotation about the same axis. v_r denote the circular velocity of any point A on the rotor with respect to the stator. The direction of a_k is radial (according to the right-hand rule), with a value equal to $2\omega v_r$. When v_r fluctuates, a radial vibration will occur at of point A. However, if the actual structure of the rotor can be designed to be uniformly and symmetrically distributed along the circumference then a_k of any two symmetrical points is equal in value and opposite in direction. Therefore, the corresponding inertial forces are balanced in total. and a_k has no substantial impact on the motion or output torque of the actuator.

5. A Case of Active Torsional Vibration Control Test

We built a test bench for active torsional vibration control by using a marine diesel engine, as shown in Figure 7. The output shaft of the diesel engine was equipped with an elastic coupling. The entire testing assembly was mechanically rigid and mounted to the test bench. The connection shafts were carefully aligned. The actuator was fixed on a support through a pair of bearing pedestals, and the support was fixed on the foundation of the test bench. A full bridge strain gauge (in the direction of 45° and 135°to the axis) was pasted on the connecting shaft between the actuator and the dynamometer to measure the dynamic torque signal of the shaft system [26], revealing the torsional vibration characteristics of the shaft system and the suppression effect as the error signal of active control. The Hall-type speed sensor was used to measure the engine speed as the reference signal for active control. Figure 8 and Figure 9 show the actual layout of the strain gauge and speed sensor, respectively.

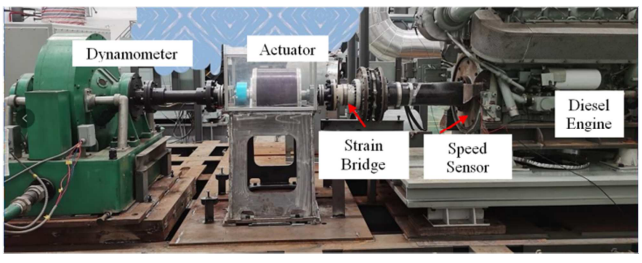

Figure 7. *Torsional Vibration Active Control Test Bench.*

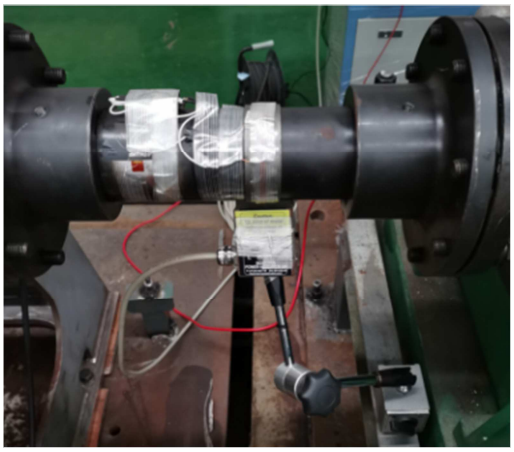

Figure 8. *Strain Bridge and Telemetry Module.*

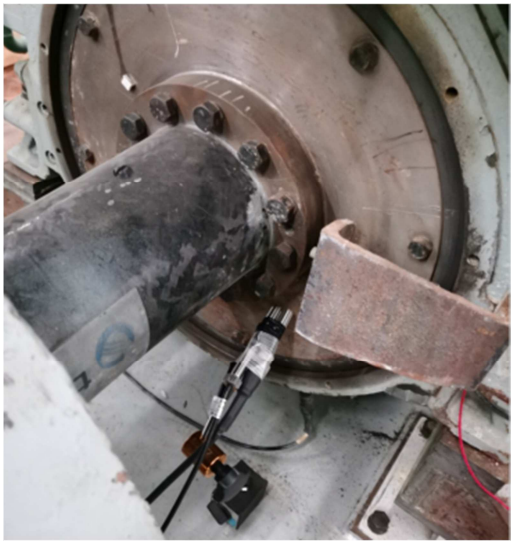

Figure 9. *Speed Sensor and Inductive Magnet Piece.*

The active control system was mainly composed of a control module, power amplifier, torsional vibration sensor, speed sensor, and control software, etc. The block diagram of the control system is shown in Figure 10.

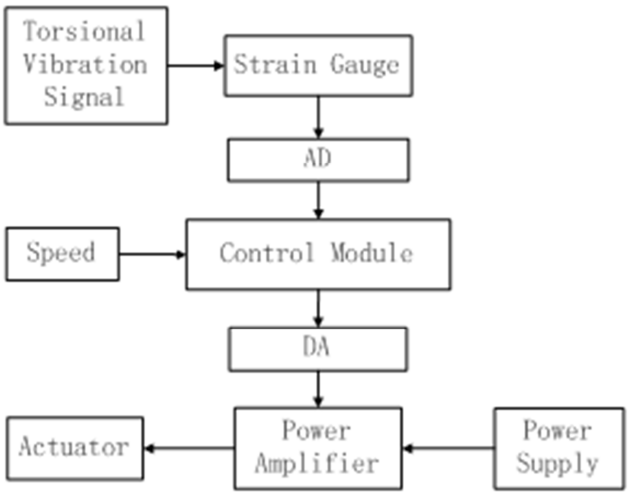

Figure 10. *Block Diagram of Active Control System.*

The active control software adopted the adaptive filtering feed forward FxLMS (Least Mean Square) algorithm, and the algorithm block diagram is shown in Figure 11.

LMS system of Siemens Company and Pulse system of B&K Company were used for test instruments. The torsional vibration signal of the strain gauge was expressed in units of torque. The dynamic torque output by the actuator was measured by the same point. The relevant results of the test were as follows:

(1) The torsional vibration frequency spectrum of the shafting of the diesel engine under operation shown in Figure 12 displays several peaks while the dynamic actuator is inactive.

(2) Figure 13 depicts the single frequency dynamic torque time domain data from the actuator outputs when the diesel engine is inactive. According to the main frequency components of diesel engine torsional vibration shown in Figure 12, Figure 13 lists the actuator output dynamic torque time domain signals at the corresponding frequencies. The excitation electric current peaks provided by the power amplifier were 6-8A. Comparing the amplitudes of the two, the output torque of the actuator can completely cover the torsional vibration of the shafting excited by the torque fluctuation from the diesel engine.

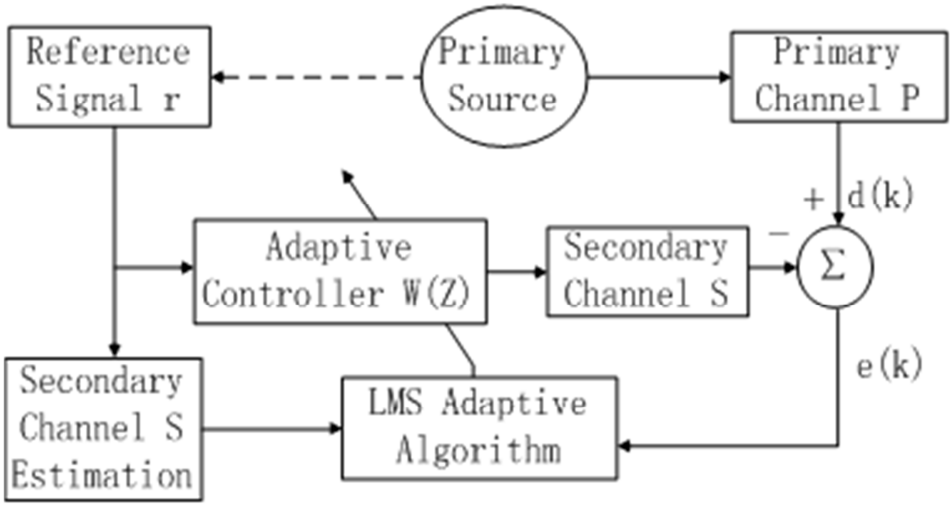

Figure 11. *Block Diagram of Active Control Algorithm.*

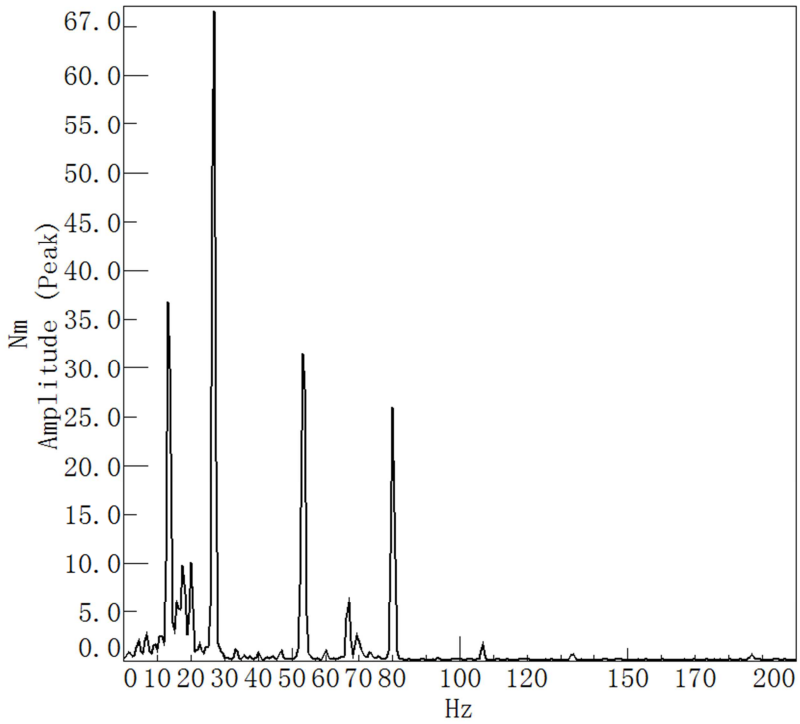

Figure 12. *Torsional Vibration Spectrum of Shafting under stable Operation of Diesel Engine at 800 rpm.*

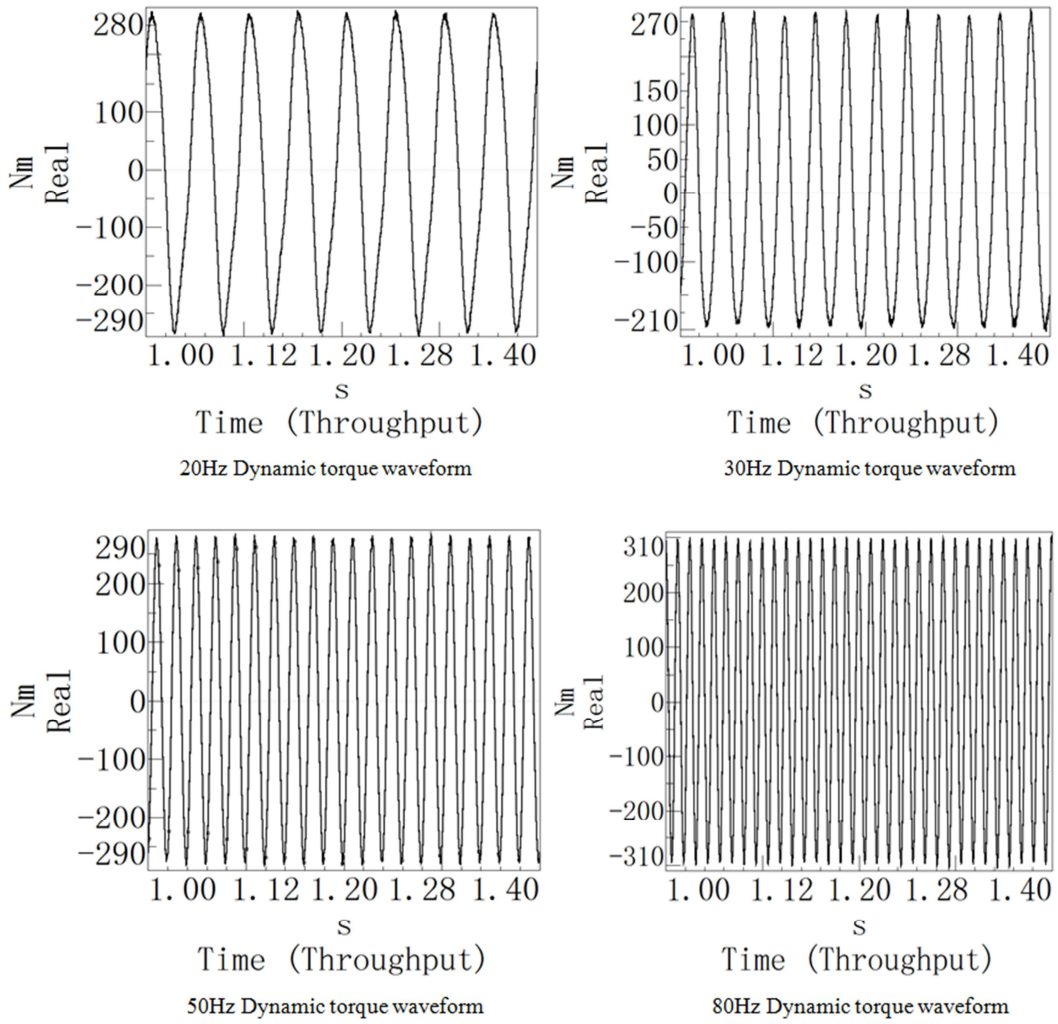

Figure 13. *Single Frequency Output Torque Time Domain Signals of Actuator.*

(3) The effect of the actuator on torsional vibration active control as the diesel engine ran under stable operation.

The data in Figure 14 are summarized in Table 1. As shown in Table 1, the suppressive effects on the torsional vibrations at 4 frequencies are from about 15dB to 26dB.

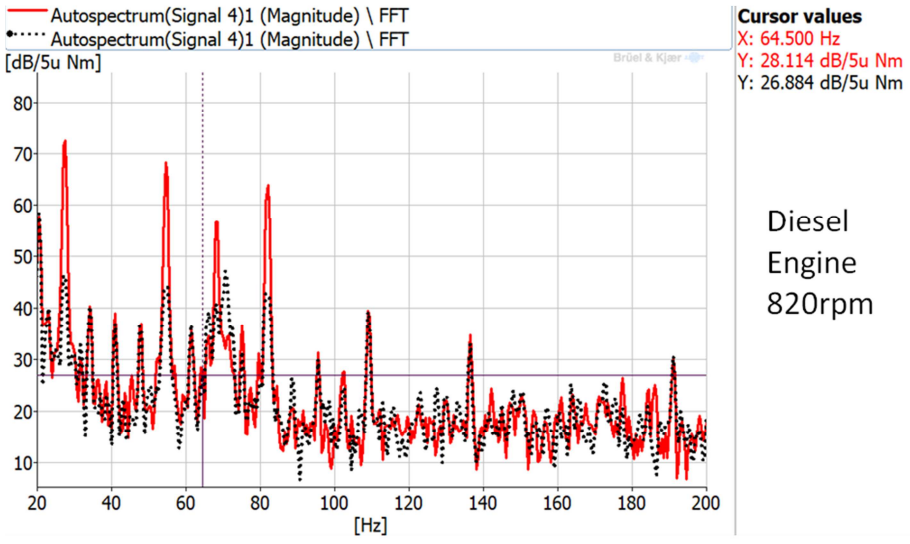

Figure 14. *Comparison of Torsional Vibration Power Spectrum between before and after Active Control (solid line - before control, dotted line - after control; reference value: 5μNm).*

Table 1. *Torsional Vibration Active Control Effect (Diesel Engine 820rpm) [27].*

Frequency/Hz	27.5	54.5	68	82
Engine Speed Harmonic	2	4	5	6
Level Before Control/dB	72.6	68.3	56.6	63.9
Level After Control/dB	45.9	43.6	40.9	42.3
Effect/dB	26.7	24.7	15.7	21.6

6. Conclusion

This paper introduces a set of new methods for active control of harmonic torsional vibration of shafting caused by diesel engines, propellers, and other excitation sources. This includes:

(1) A multi-body dynamic model of a complex shafting assembly is built to analyze the spatial movement (vibration) of multiple degrees of freedom with constraints, combining rigid body with elastic finite element. The calculation of the simulation model can reveal the coupling characteristics of the torsional vibration and the motion/vibration in other directions. Therefore, the suppression of the torsional vibration should also reduce the coupled vibrations as well. That indicates a path for designing and optimizing the active control of torsional vibration.

(2) A new multi-channel harmonic adaptive global control algorithm with cross-coupling control channels presents an effective solution for deploying multiple active control actuators in complex shafting assemblies.

(3) An innovative type of dynamic torque actuator, which can rotate with the coaxial shaft at high speed, and at the same time provide dynamic torque in a wide frequency range, combined with the active control system, can solve the multi-narrow-band spectral line torsional vibration caused by excitation sources. This approach shows promise to reduce harmonic torsional vibration for engines and other power systems.

Data Availability Statement

The datasets used and/or analyzed during the current study are available from the corresponding author uponon reasonable request.

References

[1] YANG Fan, Causes and Countermeasures of Torsional Vibration of Ship Shafting, Internal Combustion Engine & Parts 90 (2017) 90.

[2] Khin Khin Moe. Effect of Propeller Tip Clearance on Ship Hull Excited Force Induced by Propeller [D], 2007: 6-7.

[3] ZHANG Zhaozhen, Study on Magnetorheological Fluid Torsional Vibration Damper Based on Engine Crankshaft System, Jiangsu University, Jiang Su, 2017 53-60.

[4] JIA Feng, WANG Ruiming, LI Zheng, et al., Torsional Vibration Active Disturbance Rejection Control of Wind Turbine Generator Shafting under Grid Faults, Electric Power Automation Equipment 35 (2015) 76-77.

[5] WANG Yang, MA Zedong, ZHANG Baozhi, et al. Multibody Dynamics Modeling and Dynamic Response Analysis of the Heavy Duty Diesel Engine. Vehicle & Power Technology, 2022, 165 (1): 23.

[6] Widrow B, Glover J R, McCool J M, et al. Adaptive noise cancelling: Principles and applications [J]. Proceedings of the IEEE, 1975, 63 (12): 1692-1716.

[7] Morgan D. An analysis of multiple correlation cancellation loops with a filter in the auxiliary path [J]. IEEE Transactions on Acoustics, Speech, and Signal Processing, 1980, 28 (4): 454-467.

[8] Elliott S, Stothers I, Nelson P. A multiple error LMS algorithm and its application to the active control of sound and vibration [J]. IEEE Transactions on Acoustics, Speech, and Signal Processing, 1987, 35 (10): 1423-1434.

[9] Cabell R, Palumbo D, Vipperman J. A principal component feedforward algorithm for active noise control: Flight test results [J]. IEEE Transactions on Control Systems Technology, 2001, 9 (1): 76-83.

[10] Chang D C, Chu F T. Feedforward active noise control with a new variable tap-length and step-size filtered-x LMS algorithm [J]. IEEE/ACM transactions on audio, speech, and language processing, 2014, 22 (2): 542-555.

[11] Kim S, Park Y. Active control of multi-tonal noise with reference generator based on on-line frequency estimation [J]. Journal of sound and vibration, 1999, 227 (3): 647-666.

[12] Zhang Z Y, Hu F, Hua H X. Simulation and experiment on active vibration isolation with an adaptive method [J]. Proceedings of the Institution of Mechanical Engineers, Part M: Journal of Engineering for the Maritime Environment, 2010, 224 (3): 225-238.

[13] Ahmed A. Shabana. Dynamics of Multibody Systems. Cambridge University Press, 2005.

[14] Qi-an Peng, Sanmin Wang, Changjian Zhi, et al. A New Flexible Multibody Dynamics Analysis Methodology of Deployable Structures with Scissor‐Like Elements. Chinese Journal of Mechanical Engineering, 2019, 32 (1): 2-4.

[15] SHEN Kang-li, LUO Shuai, YANG Hao, et al. Influence of Node Connection Relationship on Structual Stiffness Matrix. Proceedings of the 28th National Conference on Structrual Engineering (No. I), 2019, Engineering mechanics: 228-232.

[16] H. Y. Isaac Du, Jeff Morgan, Jason M. Wong, et al. Modeling and Correlation of Driveshaft Whirl Dynamics for RWD Sport Utility Vehicles. SAE Paper No. 2001-01-1503, 2001: 2-4.

[17] WANG Chaoyang. Research of The Vehicle Front Wheelangle Measrement Based on The Gyroscope [D], 2015: 15-19.

[18] H. Y. Isaac Du, Xiangming Fang, Jia-Shiun Chen, et al. Modeling and Simulation of Torsional Vibration of the Compliant Sprocket in Balance Chain Drive Systems. SAE Paper No. 2008-01-1529, 2008: 4.

[19] TIAN Changhui, LEI Humin, ZHU Changchun, et al.,Stability of the Shaking Table Fixed in Tangent Direction of the Centrifuge. Machine Tool & Hydraulics, 2002 (5): 14-15.

[20] Edward J. Haug. Computer Aided Kinematics and Dynamics of Mechanical Systems Vol. I Basic Methods. Allyn and Bacon, 1989 (chinese translation): 69-71.

[21] H. Y. Isaac Du. Simulation of Flexible Rotating Crankshaft with Flexible Engine Block and Hydrodynamic Bearings for a V6 Engine. SAE Paper No. 1999-01-1752, 1999: 4-6.

[22] HUANG Ying, LING Qiang, ZHANG Fu-jun, et al. Influencing Mechanism of Fuel Injection Vector on Diesel Engine Torsional Vibration. Transactions of CSICE, 2012, 30 (1): 63-65.

[23] LUO Qing, HAN Jing, LEI Lei, SONG Endong, Introduction of the Electric Torsional Vibration Exciter and Its Application in Vibration Modal Test of Driveline Systems, Noise and Vibration Control 40 (2020): 244.

[24] Shanghai Marine Diesel Engine Research Institute, An Automatic Control Device for Restraining Torque Fluctuation, CN113809871A, China, 2020-06-11.

[25] LUO Qing, FANG Jian, DENG Youbi, YIN Gang, Comparison Among Several Mass-spring Dampers and Their Applications on Interior NVH, 2008 SAE-CHINA CONGRESS PROCEEDINGS (Volume I), 2008: 418-419.

[26] HU Bin, LIU Wei, JIANG Mingyong, WANG Weici, ZHOU Yan, Direct Measurement Method on Dynamic Torque of Power Plant, Diesel Engine 27 (2005): 31.

[27] FAN Wenkun, HU Jie, Test Report on Active Control of Torsional Vibration [R], Shanghai Marine Diesel Engine Research Institute, 2021.